Fermi-level oscillation in *n*-type *δ*-doped Si: A self-consistent tight-binding approach

X. Cartoixà* and Y. -C. Chang
Department of Physics, University of Illinois at Urbana-Champaign, Urbana, Illinois 61801, USA
(Received 2 May 2005; revised manuscript received 19 July 2005; published 20 September 2005)

We have used the empirical tight-binding method within the antibonding orbital model to compute the self-consistent potential profile and Fermi level position in *n*-type *δ*-doped Si. This model describes the six valleys in the Si conduction band adequately. We include exchange-correlation effects under the local density approximation. The comparison of our results to empirical pseudopotential calculations shows very good agreement, while effective mass approximation calculations agree only in the low doping regime. At ultra high densities, an oscillatory behavior of the Fermi-level position as a function of the doping concentration is predicted.

DOI: 10.1103/PhysRevB.72.125330 PACS number(s): 73.21.Cd, 71.20.Mq, 71.15.−m

I. INTRODUCTION

Nowadays, *δ*-doping layers are widely used in electronic devices. Apart from their role as suppliers of carriers for two-dimensional electron gases (2DEGs),[1] or two-dimensional hole gases (2DHGs),[2] they can also be employed both as contact and channel in a field effect transistor,[3] as a barrier in double barrier resonant tunneling devices,[4] as contacts in an interband tunnel diode,[5] as well as improve the characteristics of a heterojunction bipolar transistor.[6]

With the recent achievement of very high P concentration in *δ*-doped Si and its proposed use for quantum computation[7,8] and epitaxial circuitry,[9] the theoretical study of these ultra-high concentration layers in Si has become more important.

Because of its ease of implementation and low computational requirements, most of previous theoretical studies of *δ*-doping layers in Si have used the effective mass approximation. Eisele[10] and Li *et al.*[11] computed the *n*-type potential profile of a single layer with a simple model. Scolfaro *et al.*[12] have studied the electronic structure of superlattices with a multivalley effective mass approximation formalism. One drawback of the effective mass approximation is that it fails to describe properly the intervalley couplings introduced by the self-consistent confining potential, although this can be remedied to some extent with the introduction of further parameters.[12] On the other hand, an atomistic method such as empirical tight binding[13] will take into account automatically the effect of the reduced symmetry, but until present it has only been applied to *p*-type *δ*-doped semiconductors.[14]

In this work we present a self-consistent tight binding calculation of the electronic structure of a *n*-type *δ*-doped Si. It is found that at ultra-high doping concentrations, the Fermi level as a function of the doping density has an oscillatory behavior. The understanding of such an oscillatory behavior is important for the design of ultra-high density epitaxial circuitry and quantum information devices. The paper is organized as follows. In Sect. II we present the antibonding orbital model (ABOM) used and the computational methods we employ. Then, in Sec. III we show and analyze our results, comparing them with effective mass approximation and empirical pseudopotential calculations. Finally, we show our conclusions in Sec. IV.

II. METHODS

The results presented here are obtained with the empirical tight binding method.[13] We chose a basis composed of $\{|s\rangle,|p_x\rangle,|p_y\rangle,|p_z\rangle\}$ antibonding (conduction band) states located on a fcc lattice, following the antibonding orbital model (ABOM) by Chang *et al.*[15] This basis describes the bands that originate from the conduction band $\Gamma_{2'}$ and Γ_{15} states[16] at the zone center. Since this is a full zone model, it will include in the formalism the effects caused by the intervalley mixing arising from the reduced D_{2d} symmetry of the *δ* layer. Second-neighbor couplings are kept to describe properly the Δ line valleys. The reduced dimensionality of the ABOM basis allows for faster calculations with respect to atomic orbital-type tight binding calculations.[17]

The matrix elements of the Hamiltonian H are given by the following set of parameters:

$$\begin{aligned}
&\langle \mathbf{R}_0,s|H|\mathbf{R}_0,s\rangle = E_s \quad \langle \mathbf{R}_0,p_x|H|\mathbf{R}_0,p_x\rangle = E_p \\
&\langle \mathbf{R}_0,s|H|\mathbf{R}_1,s\rangle = E_{ss} \quad \langle \mathbf{R}_0,s|H|\mathbf{R}_2,s\rangle = V_{ss} \\
&\langle \mathbf{R}_0,s|H|\mathbf{R}_1,p_x\rangle = E_{sx} \quad \langle \mathbf{R}_0,s|H|\mathbf{R}_2,p_x\rangle = V_{sx} \\
&\langle \mathbf{R}_0,p_x|H|\mathbf{R}_1,p_x\rangle = E_{xx} \quad \langle \mathbf{R}_0,p_z|H|\mathbf{R}_1,p_z\rangle = E_{zz} \\
&\langle \mathbf{R}_0,p_x|H|\mathbf{R}_1,p_y\rangle = E_{xy} \quad \langle \mathbf{R}_0,p_y|H|\mathbf{R}_2,p_y\rangle = V_2 \\
&\langle \mathbf{R}_0,p_x|H|\mathbf{R}_2,p_x\rangle = V_1 + V_2, \qquad (1)
\end{aligned}$$

and the rest of the matrix elements can be obtained by application of the corresponding symmetry operations.

The parameters for our calculations are obtained from Ref. 15. Since we are ready to sacrifice full zone accuracy in favor of more precision in the description of the bands near the conduction band (CB) edge, where the occupied states will lay, we choose the parameter set labeled with Si (II). For completeness, we include the employed parameters in Table I.

The expression of the Hamiltonian matrix elements with nearest and second-nearest neighbors allows for a fast diagonalization of the Hamiltonian matrix, since it possesses a high degree of sparseness. For large problems a sparse, itera-

TABLE I. Parameters used for Si in the antibonding orbital model.

E_s	5.35359
E_p	10.29167
E_{ss}	0.18938
E_{sx}	0.1365792
E_{xx}	0.1375
E_{zz}	−2.873505
E_{xy}	0.6049156
V_{ss}	−0.57935
V_{sx}	0.07792
V_1	−0.713766
V_2	0.808316

tive method of diagonalization requiring matrix-vector products only (e.g., ARPACK[18]) is preferred, specially as the physical model we employ leads to requesting only a few (typically in the range 10–20) lowest eigenvalues of the spectrum of the Hamiltonian. The iterative methods have the added advantage of requiring very little storage because the matrix-vector products can be straightforwardly expressed in terms of the 19 (one on-site, 12 nearest-neighbors, six second-nearest-neighbors) 4×4 coupling matrices.

The self-consistency cycle is started with the specification of a guess to the sum of the Hartree potential $V_H(z)$ and a local approximation $V_{XC}(z)$ to the exchange-correlation potential. Then the Schrödinger equation

$$\left[H(\mathbf{k}_\parallel) + V_H(z) + V_{XC}(z)\right]\psi_{n,\mathbf{k}_\parallel}(z) = E_n(\mathbf{k}_\parallel)\psi_{n,\mathbf{k}_\parallel}(z) \quad (2)$$

is solved, where $H(\mathbf{k}_\parallel)$ is the bulk ABOM Hamiltonian and $E_n(\mathbf{k}_\parallel)$ is the energy of the nth level $\psi_n(z)$ at the reciprocal space point $\mathbf{k}_\parallel$. $V_H(z)$ and $V_{XC}(z)$ are taken as diagonal in the ABOM basis set. Then, the effective mass corresponding to each level m_n^* is calculated and the charge density is computed using

$$\rho(z) = \frac{2}{a\pi\hbar^2}\times\left(\sum_n m_n^*|\psi_{n,0}(z)|^2\int_{E_n(0)}^{\infty} f_{\mathrm{FD}}(E;\mu,T)dE + 4\sum_{n'} m_{n'}^*|\psi_{n',\mathbf{k}_{\min}}(z)|^2\int_{E_{n'}(\mathbf{k}_{\min})}^{\infty} f_{\mathrm{FD}}(E;\mu,T)dE\right), \quad (3)$$

where a is the unit cell size, $\mathbf{k}_{\min}$ is the position of one of the four degenerate valleys in the k_x-k_y plane, $f_{\mathrm{FD}}(E;\mu,T)$ is the Fermi-Dirac distribution for a chemical potential μ and a temperature T, and n, n' run through the levels with energies less than $\mu+10k_BT$, with k_B being the Boltzmann constant. Note that we do not include a factor of two in front of the contribution to the charge density from the zone center states because the folding of the two valleys with $k_z\neq0$ onto the zone center and the coupling of these two valleys is automatically included in our model. Then we solve the Poisson equation to obtain $V_H(z)$ for the following iteration, and the exchange-correlation potential in the local density approximation is computed from $\rho(z)$ from the parametrization by Perdew and Zunger.[19] We stop the cycle when the maximum relative change in $V_H(z)+V_{XC}(z)$ between iterations is less than 10^{-3}. We find that using the Pulay mixing scheme[20,21] convergence improves greatly with respect to linear mixing, specially at medium and high charge densities.

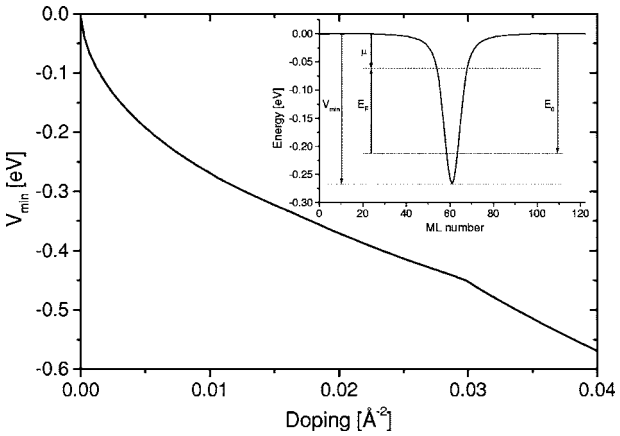

FIG. 1. Minimum of the self-consistent potential for a n-type δ layer. The full width half maximum (FWHM) of the donor distribution is 16.0 Å. The inset illustrates several symbols used in the text (all quantities are negative except for E_F) for a potential profile corresponding to a carrier concentration of 9.82×10^{-3} Å^{-2}.

The background charge is modeled by a Gaussian distribution. The energy difference between the Fermi level and the first bound state is set as an input parameter. Charge neutrality is ensured at each iteration step by rescaling the donor background concentration to match the electron concentration. This procedure avoids the trial of several Fermi levels until achievement of charge neutrality.

Normally, we are interested in the position of the Fermi level with respect to the conduction band edge (CBE) for a series of concentrations. As previously mentioned, we sweep the concentrations by changing the energy separation between the Fermi-level μ and the first bound state E_0. This separation is defined as $E_F\equiv\mu-E_0$. Figure 1 shows the depth of the self-consistent potential as a function of dopant density. It is found that the potential minimum decreases monotonically as the density increases. Due to the approximate linearity seen in Fig. 1 we have found that, during a ramp up of E_F, the extrapolation of the two previous potential profiles yields a very good guess for the value of E_F at which calculations are being made, requiring only approximately ten iterations to reach convergence even for the highest density considered.

III. RESULTS

A. Exchange-correlation effects

In our calculations, the exchange-correlation effect is included within the local density approximation (LDA). As shown in Fig. 2, the inclusion of the exchange-correlation (XC) terms changes the results significantly with respect to calculations with Hartree terms only. The observed changes

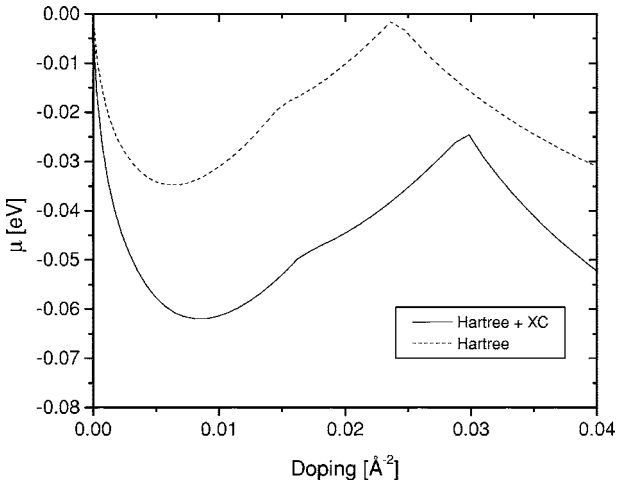

FIG. 2. Position of μ as a function of the doping for a FWHM of the dopant distribution of 16.0 Å with (solid) and without (dashed) exchange-correlation terms, at 0 K.

in the positions of the energy levels and the Fermi level, of a few tens of meV are in qualitative agreement with previous density functional calculations in Si interfaces[22] and recent empirical pseudopotential results.[23] Here we choose a full width half maximum (FWHM) for the donor distribution of 16.0 Å, consistent with the experimental results of 15 Å in Ref. 7. For this amount of spread, the Fermi level versus doping concentration displays a minimum at doping density (n) around 0.01 Å^{-2}. Note that at low density limit, the Fermi level approaches zero, consistent with previous effective-mass model calculations. However, this is inconsistent with the fact that at zero density limit the Fermi level should coincide with the ground state energy of Si donor at 0 K, which is around −0.029 eV (Ref. 24) (no short range effects/chemical species information about the donor are included in our calculations). This obvious discrepancy is caused by the fact that the doping potential used in the calculation is averaged over the in-plane coordinates (x and y), which is a good approximation only at the high density limit when the average donor separation is smaller than the effective Bohr radius (around 25 Å for phosphorous donor in Si). To remove such discrepancy, one needs to replace the in-plane uniform doping potential by a dilute two-dimensional array of donors in the doping planes, which would require formidable computational effort. Since our main interest is in the high density limit, it suffices to study the model with an in-plane averaged doping potential with the understanding that at low doping densities the Fermi-level position should approach the donor ground state rather than zero. With this in mind, we see that the Fermi level calculated within Hartree approximation (dotted line in Fig. 2) should start at around −0.029 eV at zero density and gradually increase as the density increases. It then reaches a maximum at n around 0.024 Å^{-2}, and then decrease again, showing an oscillatory behavior. The increase of Fermi level with increasing density can be understood in terms of the screening and band filling effects. The turn-around at $n \sim 0.024$ Å^{-2} (causing an oscillatory behavior) will be explained in Sec. III C. When the exchange-correlation (XC) effect is included, it lowers the

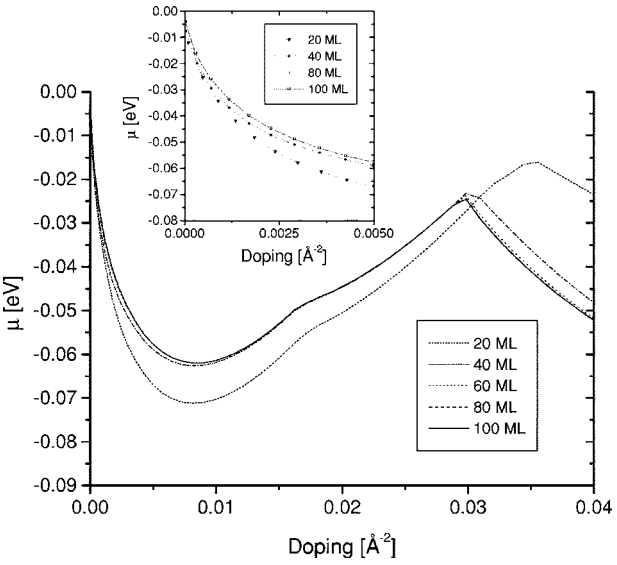

FIG. 3. Position of μ as a function of the doping for structures with different separation between the δ layers.

subband energies and hence, the Fermi level. Consequently, the Fermi level shows a minimum at $n \sim 0.01$ Å^{-2}. The XC effect also pushes the turn-around point to higher density.

B. Dependence on the size of superlattice unit cell

Since we are using periodic boundary conditions to facilitate the calculation, we need to make sure that the superlattice unit cell is large enough so that neighboring δ layers are decoupled. Figure 3 shows the position of the Fermi level μ as a function of the doping concentration for several spacer thicknesses. The full width half maximum (FWHM) for the donor distribution of 16.0 Å is assumed. We see that convergence has been achieved for a separation of 80 ML (at 2.7155 Å/ML), indicating an effective decoupling of the δ layers. This is in good agreement with Scolfaro *et al.*,[12] who found that the δ layers are decoupled at ~200 Å of separation.

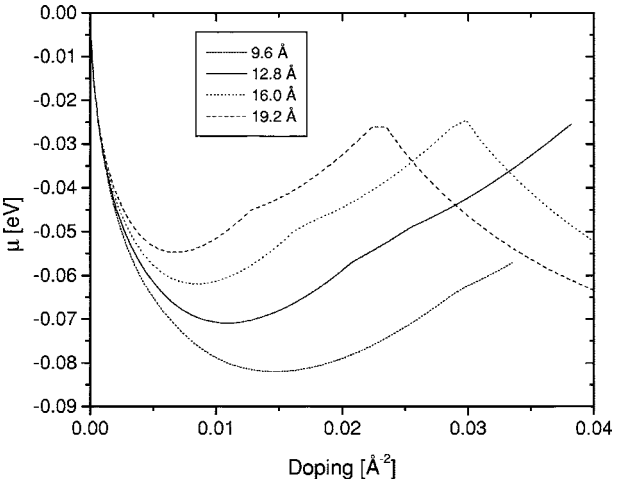

FIG. 4. Position of μ as a function of the doping for structures with different FWHM of the dopant distribution.

C. Effect of spreading of the δ-layer doping

Figure 4 shows the Fermi-level position as a function of doping density for different values of FWHM of the doping distribution. The XC effect is included here. This could model, for example, the effect of a longer annealing time after dopant deposition or the effect of a higher growth temperature.

We see that the position of the Fermi level is fairly sensitive to the value of the FWHM. In particular, we see that at lower and medium dopant concentrations, the Fermi level gets lower as the FWHM decreases. This is because the confining potential will be shallower for less concentrated dopant distributions and, therefore, the energy levels will be closer to the conduction band (CB) edge. Thus, the Fermi level will also be closer to the CB edge.

Another important feature seen in Fig. 4 is the presence of an oscillatory behavior in the Fermi level. This can be explained from the rates of change of the self-consistent energy levels as the doping is increased. In the parabolic band approximation and at 0 K, the position of the Fermi level is given by

$$\mu = \frac{Cn + \sum_{i=0}^{N-1} m_i^* E_i}{\sum_{i=0}^{N-1} m_i^*}, \tag{4}$$

where E_i is the energy of the ith level, with i running through the N occupied levels, n is the two-dimensional electron density, and $C \equiv \pi\hbar^2$ is a constant.

Taking the derivative of Eq. (4) with respect to the electron concentration—that is to say, with respect to the doping amount—we obtain, assuming the effective masses do not vary much when the concentration is changed

$$\frac{d\mu}{dn} \approx \frac{C}{\sum_{i=0}^{N-1} m_i^*} + \frac{\sum_{i=0}^{N-1} m_i^* dE_i/dn}{\sum_{i=0}^{N-1} m_i^*}. \tag{5}$$

The first term will always be positive, while the second will always be negative. This equation is easy to interpret when only the first bound state is occupied. The rate at which the energy separation between the Fermi level and the first bound state E_F will change is the inverse of the density of states C/m_0^*. Now, if E_0 decreases faster (slower) than E_F grows when the charge density augments, μ will decrease (increase). Equation (5) basically describes this same argument for the case where multiple bands are occupied. Thus, the Fermi-level position as a function of doping density will display either a kink or a turn-around when a new subband begins to get filled.

In the particular case shown in Fig. 4, the turn-around occurs when a new set of states originating from the minima along the ⟨100⟩ lines becomes low enough in energies to be occupied.

D. Finite temperature effects

Next, we study the effect that finite temperatures have on the position of the chemical potential μ. Figure 5 shows μ as a function of the doping concentration for several temperatures. We find that the variations in μ become less dramatic as temperature increases, as expected due to the thermal smearing of the occupation probabilities. The chemical potential still shows an oscillatory behavior for FWHM = 19.2 Å at 77 K.

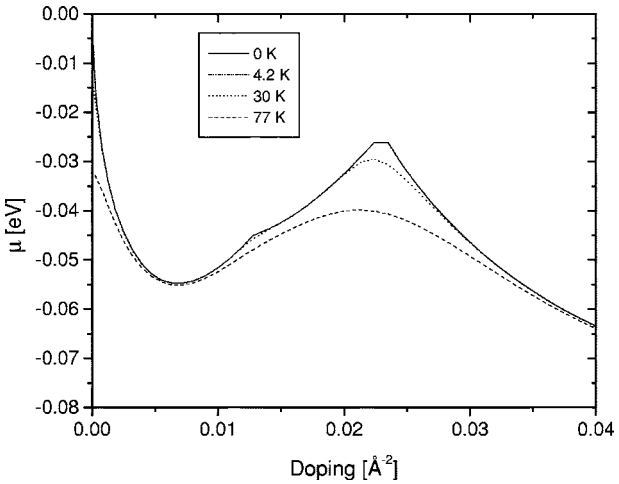

FIG. 5. Position of μ as a function of the doping for different temperatures and a FWHM of the dopant distribution of 19.2 Å.

E. Intervalley mixing and nonparabolicity effects

Since ABOM is a full zone description, intervalley mixing and band nonparabolicity are naturally included within the model. However, this same embedding makes it difficult to decouple these effects from the rest of the simulation. Thus, we resort to comparison with effective mass approximation (EMA) for this purpose.

In Fig. 6 we compare results obtained with ABOM to EMA calculations. Label EMA1 refers to calculations with the standard Si effective masses $m_t^* = 0.19$ and $m_l^* = 0.92$, while EMA2 refers to calculations with $m_t^* = 0.19$ and $m_l^* = 1.2$. The masses in EMA2 are chosen to match those obtained from the ABOM bands. Note that for high doping

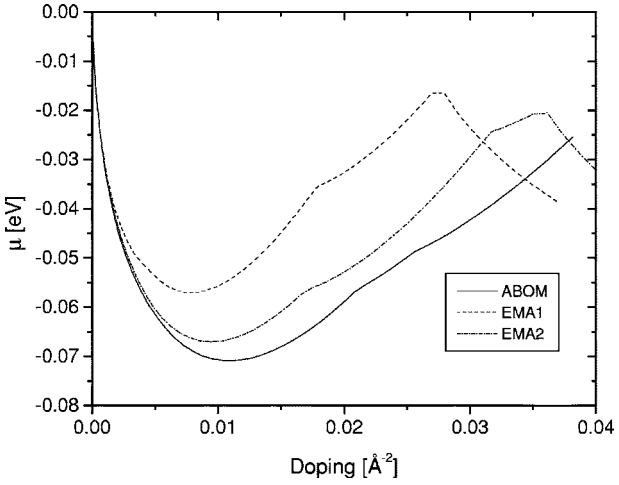

FIG. 6. Position of μ as a function of the doping for ABOM and two implementations of EMA (see text for details).

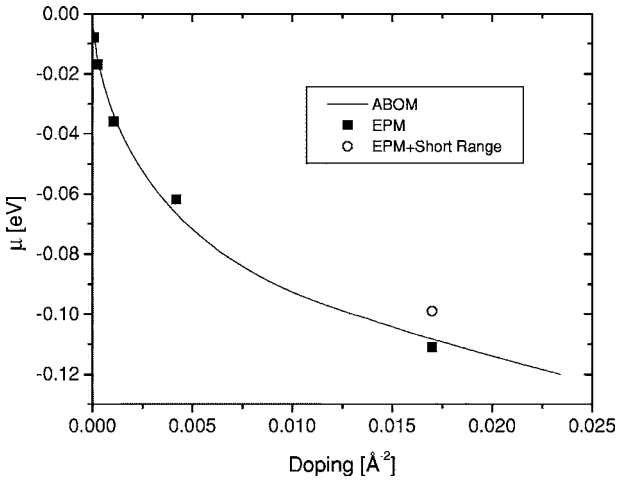

FIG. 7. Comparison of ABOM with empirical pseudopotential method (EPM) results (from Ref. 23). The open circle labels results including short range Coulomb interaction effects, while full squares do not include this correction.

concentrations, the band filling is so high that the band nonparabolicity effect will be important. Since the bandwidth for the conduction band structure along the [001] axis obtained in ABOM is in agreement with the empirical pseudopotential model, the use of an enlarged value of m_l^* as obtained in ABOM can actually give a more reliable value for the density of states on the energy scale of interest here.

We see that the biggest effect on the results comes from the use of different effective masses (EMA1 versus ABOM). The lighter the longitudinal mass, the lower the density of states and the higher the energy of the confined states, which both contribute to a higher Fermi level, as seen in the figure. When the influence of different effective masses is factored out (EMA2 versus ABOM), the results provide a measure of the effect of intervalley mixing and nonparabolicity. The EMA2 and EBOM results are similar up to $\sim 5 \times 10^{-3}$ Å^{-2}, showing the EMA calculations for this system lose validity at the very high dopant concentrations that can be present in δ layers proposed for epitaxial circuitry.[7,9]

F. Comparison to empirical pseudopotential results

In order to validate our results, we compare the calculated Fermi-level position for the case FWHM=0 Å to that obtained with an empirical pseudopotential method (EPM) by Qian *et al.*[23] (see their Tables I and II). Figure 7 shows an excellent agreement when the short range (SR) Coulomb interaction effects are not included in EPM (full squares), as it should be since SR terms are not included in our calculation, either. The empty circle in Fig. 7 corresponds to the inclusion of SR effects for 1/4 ML doping concentration, which reduce the position of the Fermi level by about 10%. This comparison shows that ABOM can be used reliably over the full range of technologically important doping concentrations, including the ultra-high concentration case.

IV. CONCLUSION

In conclusion, we have used an antibonding orbital model (ABOM) to calculate self-consistently the Fermi-level position for several *n*-type δ-doping structures. The use of this model has allowed us to compute the properties of δ-doped Si at ultra-high densities, of importance for possible use in epitaxial circuitry, while including the intervalley mixing and nonparabolicity effects, not available in simpler models. We have found the appearance of an oscillatory behavior in the Fermi level and related it to the behavior of the energy levels as the doping amount varies. When the temperature is raised from zero, these oscillations dampen and, in average, the Fermi level lowers to avoid a too high number of occupied bands. Such an oscillatory behavior may be of importance in the design of ultra-high density epitaxial circuitry and quantum information devices. We have shown that the exchange-correlation effects are non-negligible. Our results show very good agreement with empirical pseudopotential results while keeping a low computational cost, demonstrating the suitability of our approach for reduced dimensionality heterostructures.

ACKNOWLEDGMENTS

The authors would like to thank B. H. Lee and D. Z.-Y. Ting for helpful discussions. This work has been supported by DARPA under Contract No. DAAD19-01-1-0324.

*Present address: Department d'Enginyeria Electrònica, Universitat Autònoma de Barcelona, 08193 Bellaterra, Barcelona, Catalonia, Spain. Electronic address: Xavier.Cartoixa@uab.es

[1] E. F. Schubert, J. E. Cunningham, W. T. Tsang, and G. L. Timp, Appl. Phys. Lett. **51**, 1170 (1987).
[2] J. Wagner, A. Fischer, and K. Ploog, Appl. Phys. Lett. **59**, 428 (1991).
[3] E. F. Schubert, J. E. Cunningham, and W. T. Tsang, Appl. Phys. Lett. **49**, 1729 (1986).
[4] M. R. Sardela, H. H. Radamson, and G. V. Hansson, Appl. Phys. Lett. **64**, 1711 (1994).
[5] K. D. Hobart, P. E. Thompson, S. L. Rommel, T. E. Dillon, P. R. Berger, D. S. Simons, and P. H. Chi, J. Vac. Sci. Technol. B **19**, 290 (2001).
[6] H. R. Chen, C. H. Huang, C. Y. Chang, C. P. Lee, K. L. Tsai, and J. S. Tsang, IEEE Electron Device Lett. **15**, 286 (1994).
[7] T. C. Shen, J. Y. Ji, M. A. Zudov, R. R. Du, J. S. Kline, and J. R. Tucker, Appl. Phys. Lett. **80**, 1580 (2002).
[8] L. Oberbeck, N. J. Curson, M. Y. Simmons, R. Brenner, A. R. Hamilton, S. R. Schofield, and R. G. Clark, Appl. Phys. Lett. **81**, 3197 (2002).
[9] J. R. Tucker and T. -C. Shen, Solid-State Electron. **42**, 1061 (1998).
[10] I. Eisele, Superlattices Microstruct. **6**, 123 (1989).
[11] H. M. Li, K. F. Berggren, W. X. Ni, B. E. Sernelius, M. Willander, and G. V. Hansson, J. Appl. Phys. **67**, 1962 (1990).

[12] L. M. R. Scolfaro, D. Beliaev, R. Enderlein, and J. R. Leite, Phys. Rev. B **50**, 8699 (1994).
[13] J. C. Slater and G. F. Koster, Phys. Rev. **94**, 1498 (1954).
[14] L. M. Gaggero-Sager, S. Vlaev, and G. Monsivais, Comput. Mater. Sci. **20**, 177 (2001).
[15] Y. -C. Chang, A. E. Chiou, and M. Khoshnevissan, J. Appl. Phys. **71**, 1349 (1992).
[16] O. E. Madelung, *Semiconductors – Basic Data* (Springer-Verlag, Berlin, Germany, 1996), 2nd ed.
[17] P. Vogl, H. P. Hjalmarson, and J. D. Dow, J. Phys. Chem. Solids **44**, 365 (1983).
[18] R. Lehoucq, K. Maschhoff, D. Sorensen, and C. Yang, ARPACK: ARNOLDI PACKAGE (1997), http://www.caam.rice.edu/software/ARPACK/.
[19] J. P. Perdew and A. Zunger, Phys. Rev. B **23**, 5048 (1981).
[20] P. Pulay, Chem. Phys. Lett. **73**, 393 (1980).
[21] G. Kresse and J. Furthmuller, Comput. Mater. Sci. **6**, 15 (1996).
[22] T. Ando, Phys. Rev. B **13**, 3468 (1976).
[23] G. Qian, Y. -C. Chang, and J. R. Tucker, Phys. Rev. B **71**, 045309 (2005).
[24] W. Kohn and J. M. Luttinger, Phys. Rev. **98**, 915 (1955).